

RESEARCH ARTICLE

A 1T2R High-Sensitivity and Dual-Channel Transceiver for Backscatter Communication Systems

SIJIA LAI^{ID}, YUXIAO ZHAO, (Member, IEEE), MENG LIU^{ID}, SHENGLIANG XU, KUANGFENG TANG^{ID}, AND HAO MIN^{ID}, (Member, IEEE)

State Key Laboratory of ASIC and System, School of Microelectronics, Fudan University, Shanghai 200120, China

Corresponding author: Hao Min (hmin@fudan.edu.cn)

This work was supported by the Backscatter Communication Project Between Fudan University and Huawei Technologies Company Ltd.

ABSTRACT Owing to the rapid development of the ambient Internet of Things (IoT) industry, Backscatter Communication Systems (BCS) require higher receiver sensitivity for large-scale IoT scenarios than traditional Radio Frequency Identification (RFID) systems. This paper proposes a method of using Multiple-Input Multiple-Output (MIMO) technology to compensate for reflected signals in the 920 MHz backscatter communication systems. The researcher first created a MATLAB model to verify the theoretical feasibility and then built a One-Transmitter Two-Receiver (1T2R) BCS transceiver system compatible with the EPC *global protocol* for practical verification on LabVIEW. The ITIR and 1T2R tests were conducted using the National Instrument (NI) USRP-2952R device, the directional antennas, and the standard RF electronic tags. Through the process of superimposing and utilizing the phase shift between the two reflected carriers, it has been confirmed that the overall signal strength can be enhanced from 2.2 mV to 4.13 mV and 4.37 mV (nearly reaching 4.70 mV by using two Rx antennas in ideal conditions). After calculation, this advancement increases signal strength from -40.14 dBm (when using a single Rx antenna) to -34.18 dBm (when using two Rx antennas). The improvement in signal strength can provide a gain of 5.96 dB to the backscatter communication systems. Experimental results demonstrate that utilizing MIMO technology to the backscatter communication systems can effectively enhance the sensitivity of the receiver at 920 MHz.

INDEX TERMS 1T2R transceiver, ambient Internet of Things, backscatter communication systems, radio frequency identification, multiple-input multiple-output.

I. INTRODUCTION

Radio Frequency Identification (RFID) technology acquires energy by collecting the ambient Radio Frequency (RF) signals and communicates by reflecting external RF signals [1], [2], which have low cost and low power consumption. However, their transmission distance is usually 0.1 m – 1 m. Due to the rapid development of the ambient IoT industry, traditional RFID systems gradually cannot meet the requirements of large-scale Internet of Things (IoT) applications, such as fast inventory, smart transportation, and unmanned retail [3], [4]. Therefore, in response to these problems, the Backscatter

Communication Systems (BCS) of long-range transmission, low power consumption, low cost, and ultra-long standby tags have attracted increasing attention (Fig. 1) [5], [6]. As a special wireless-powered communication network, BCS allows IoT devices to obtain energy through dedicated or ambient RF sources to power integrated circuits and send data by reflecting RF signals [7]. BCS could be considered an upgrade from traditional passive RFID systems and will be one of the key technologies of the 6th Generation (6G) and IoT applications. However, further enhancement of their transmission distance, especially for the sensitivity of the receiver, is still a great challenge [8].

How to improve the receiver sensitivity is crucial for overcoming limitations in BCS. Applying MIMO technology

The associate editor coordinating the review of this manuscript and approving it for publication was Ahmed M. Elmisyry^{ID}.

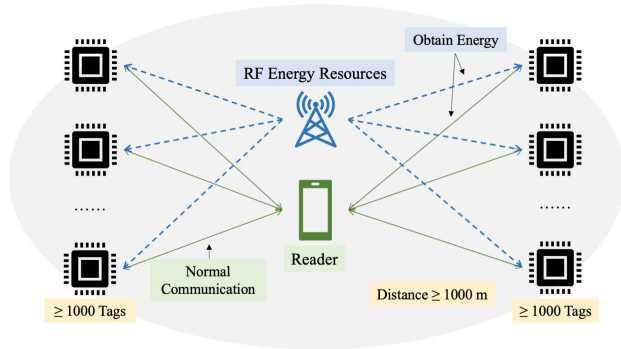


FIGURE 1. Long-transmission and multi-end backscatter communication systems for large-scale IoT applications.

to the BCS is a potential solution. MIMO technology is a well-established technology that is widely used in modern communication systems such as the 5th Generation (5G) and radar systems [9]. However, since these applications do not have high energy cost requirements, the MIMO technology has not received much attention in the RFID field. Long-range transmission and multiple-end backscatter communication systems have become an increasingly popular topic in recent years. Their communication mechanism differs from traditional cellular networks, Wi-Fi networks, and satellite networks [10], [11]. Backscatter communication technology, developed in the background of the ambient Internet of Things, can bring significant advantages to the development of smart transportation, smart agriculture, and smart logistics. It will also contribute greatly to the construction of smart cities. To make this possible, it is essential to enhance the receiving sensitivity of the backscatter communication system [12], [13], which will help extend its communication distance and increase the number of communication terminals.

In 2017, a researcher [14] attempted to study the capacity and symbol error ratio of the backscatter channel through two transmit antennas and two receive antennas to investigate the data rate and sub-channel compensation at 5.8 GHz. In the latest research in 2020, a team [15] took the lead in using mobile devices to send commands to tags, then equipped a large number of MIMO devices close to readers for signal receiving and used the minimum mean square error algorithm to evaluate communication performance. Another researcher [16] applied MIMO technology to the RFID system to improve communication robustness. The joint detection of 48 tags improved in simulation results with a BER of 20 dB at a 1/8 coding rate. The transmitter and receiver used in [17] are not part of the same device. The limited communication distance (0.1 m - 1.5 m) of the electronic tag would result in errors in the measurement. As for [14], the measurements were performed at 5.8 GHz, which is beyond the Ultra High Frequency (UHF) band, so the results of the signal gain are not helpful for BCS at 920 MHz.

After investigating several studies [18], [19], [20], [21], it has been discovered that using MIMO technology to

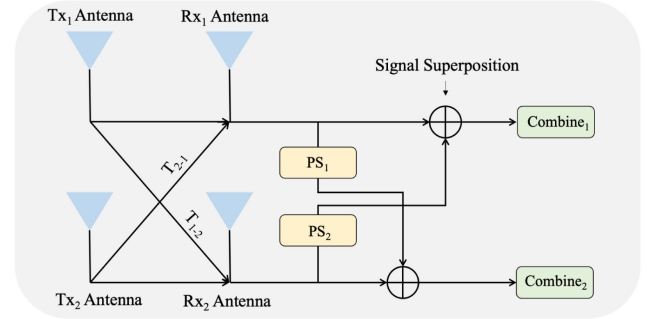


FIGURE 2. Signal transmission principles for the transceiver system.

compensate for long-distance transmission path loss is a relatively innovative application in backscatter communication. Therefore, the primary objective of this paper is to explore the theoretical feasibility and practical verification of utilizing MIMO technology in BCS within the 920 MHz frequency band.

To achieve the research objective, in Section II, the paper explains the feasibility of implementing MIMO technology to backscatter communication systems based on principles and simulates it through MATLAB. After that, a One-Transmitter Two-Receiver (1T2R) transceiver is built to support the BCS signal transmission link on the LabVIEW platform. In Section III, the NI USRP-2952R device is used as the signal source, and directional antennas and RF standard tags are added for joint testing. The signal strength is measured in both single and dual Rx antenna situations for subsequent comparison experiments. In Section IV, the MIMO technology is used to receive and superimpose the reflected signals with varying phase shifts. The experimental results confirm that the application of MIMO technology to the 920 MHz BCS can provide an energy compensation of approximately 6 dB for the receiver in both two combined channels.

II. SYSTEM DESIGN

In this section, we will discuss the theoretical feasibility of utilizing MIMO technology in backscatter communication systems and showcase this through a MATLAB model. Furthermore, we designed and constructed a transceiver that supports the BCS signal transmission link on the LabVIEW platform, laying the foundation for subsequent tests.

A. SYSTEM PRINCIPLES

The schematic diagram of the transceiver system design is shown in Fig. 2. The phase shifts need to be added in both two channels to constitute the combined signal links.

$Combine_1$ and $Combine_2$ indicate the two superimposed signals after phase shifting:

$$Combine_1 = (Tx_1 + T_{2-1}) + [(Tx_2 + T_{1-2}) + PS_2] \quad (1)$$

$$Combine_2 = (Tx_2 + T_{1-2}) + [(Tx_1 + T_{2-1}) + PS_1] \quad (2)$$

where Tx_1 , Tx_2 , T_{1-2} , and T_{2-1} are transmitting signals. PS_1 and PS_2 are phase shifting added to each signal link. For

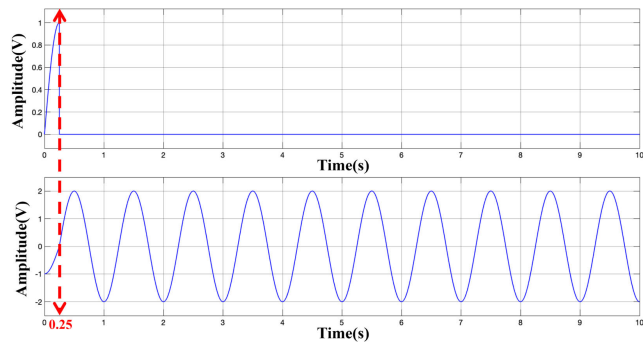


FIGURE 3. Signal simulation waveforms of the simplified receiver in MATLAB.

the received two carrier signals, if they satisfy (3), the two received signals will cancel each other out:

$$Combine_1 = \sin \omega t + \sin [\omega t - (2k + 1) \cdot \pi] = 0 \quad (3)$$

If the two reflected signals are superimposed on each other, they will meet condition (4) as follows:

$$\begin{aligned} Combine_2 &= \sin(\omega t - 2k \cdot \pi) + \sin(\omega t - 2k \cdot \pi) \\ &= 2 \cdot \sin(\omega t - 2k \cdot \pi) \end{aligned} \quad (4)$$

The signal transmission model is simulated in MATLAB R2021b. Fig. 3 indicates the time domain waveforms of the receiving combined signals 1 and 2. In order to facilitate the observation and capture of the signal, the sinewaves are set to have an amplitude of 1, an oscillation period of 1 and a frequency of $\pi/2$. The initial signal 0 is kept constant, the initial signal 1 is set to have a phase shift of $-\pi/2$. Then the two signals are given a delay of 0.25 by the modules PS_1 and PS_2 respectively.

$$\begin{aligned} Combine_1 &= \sin t + \sin(t - \pi) \\ &= \sin t - \sin t \\ &= 0 \end{aligned} \quad (5)$$

$$\begin{aligned} Combine_2 &= \sin(t - \pi/2) + \sin(t - \pi/2) \\ &= 2 \cdot \sin(t - \pi/2) \end{aligned} \quad (6)$$

The amplitude of $Combine_1$ drops to 0 at $T = 0.25$ when the two waveforms cancel each other, while the amplitude of $Combine_2$ changes from 1 to 2 when the signals are superimposed. Phase shifting could enhance and cancel reflected signals under the same signal period.

This principle of superimposed enhancement and cancellation can be illustrated in Fig. 4. If two carriers need to be superimposed and enhanced to a maximum value, their timing needs to be perfectly synchronized or differ by a multiple of the same period T . Conversely, if two carriers differ by a multiple of $T/2$, the signal gets cancelled out.

When multiple directional antennas are used to receive and combine the signal, it is expected to provide a 6 dB signal gain for the BCS. Additionally, cancellation could be used to communicate with two tags at the same time. This is of great significance for achieving fast inventory applications. Through the demo prototype of the transceiver system, the

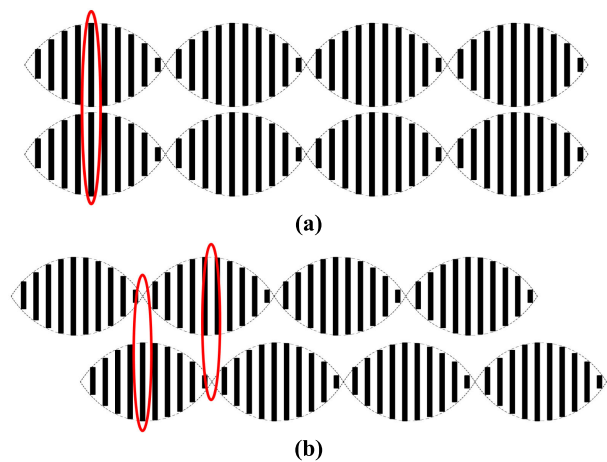


FIGURE 4. (a) Superimposed enhancement of two carriers received by the two Rx antennas. (b) Cancellation of two carriers received by the two Rx antennas.

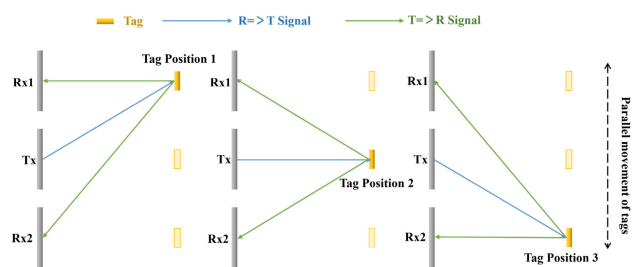


FIGURE 5. The placement of the tag and three directional antennas.

feasibility of this method can be verified as long as the enhancement and cancellation of $Combine_1$ are realized.

In the actual design of the 1T2R system, when the tag is placed at positions 1 to 3 (Fig. 5), respectively, the two Rx antennas will receive and superimpose their reflected signals separately. Because transmission distances are different, there is an inevitable signal delay. Therefore, during the tag's parallel movement, the superimposed signal's amplitude will vary and switch between enhancement and cancellation.

B. SYSTEM SIGNAL TRANSMISSION LINKS

Based on the theoretical analysis, a BCS transceiver system is built on LabVIEW. The transceiver system consists of five main parts, which are shown in red dotted circles in Fig. 6. These parts include (a) USRP device configuration, (b) Tx signal generation, (c) Tx transmission, (d) Rx receiving part, and (e) Rx signal processing. It enables communication between systems and tags, and processes reflected carriers in different channels. The USRP configuration, part (a), is primarily responsible for establishing a connection between the designed receiver system and the NI 2952R device. It also sets the specific transmission parameters of the transceiver system to drive the connection between the USRP device and the antennas. The specific parameter design is detailed in TABLE 1. In part (b) of Tx signal generation, we use the Pulse Interval Encoding (PIE) module to encode the Query Command according to protocol rules. The command is

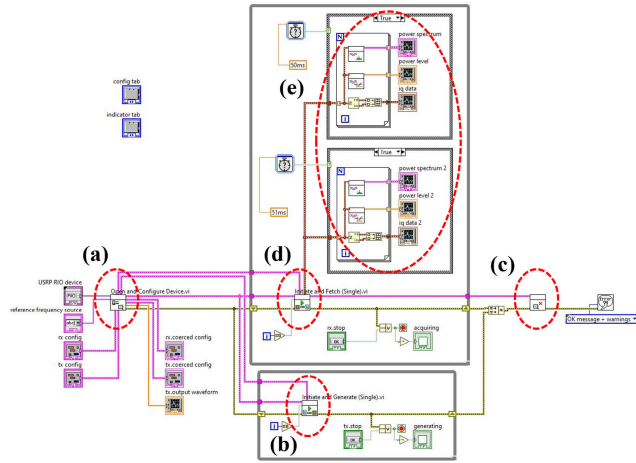


FIGURE 6. The architecture of the transceiver system built on the LabVIEW platform.

modulated, and the carrier is transmitted continuously via the Tx signal transmission part (c) according to RF transmission rules. Once the electronic tag has established communication, it will respond and reflect the signal based on the specifications [26]. At this point, the information sent by the tag can be received and collected through the Rx signal receiving part (d) and then processed and analyzed in the Rx signal processing part (e).

According to EPC global protocol, when the tag receives the correct Query Command, it reflects a 16-bit pseudorandom sequence named RN16 signal, which is a sign of successful communication between the system and the tag. Using the PIE rule, Query Command 1000110000000010001001 is sent directly to the tag. T_{tx} indicates the time length of the transmitted signal from Tx.

$$T_{tx} = T_{c1} + T_{Query} + T_{c2} \quad (7)$$

where T_{c1} and T_{c2} refer to the time length of the high-level carriers before and after the Command signal. The frequency band is set to 920 MHz under Chinese specifications, T_{ari} is 25 μs , and PW is 12.5 μs . Consequently, the overall length of the Query Command signal T_{tx} is 0.9375 ms, and the entire transmitting signal is 6.9375 ms.

$$T_{tx} = 2 \text{ ms} + 1.9375 \text{ ms} + 4 \text{ ms} = 6.9375 \text{ ms} \quad (8)$$

III. 1T2R TRANSCIVER SYSTEM

A. SYSTEM TESTING ENVIRONMENT

The USRP device is connected to a transmitting antenna, Tx, and two receiving antennas, Rx₁ and Rx₂, to set up communication with a single tag. As shown in Fig. 7. The antenna used in the test is a UHF RFID circularly polarized directional antenna with a 9 dBi gain of 260 mm * 260 mm * 30 mm size (Fig. 8. a). Their receiving area is reversely about 60° - 90° fan-shaped outward diffusion, in the center of which reaches the farthest reading distance. Meanwhile, it is necessary to keep the distance between each other more than 10 cm.

TABLE 1. Transceiver system parameter configuration.

Characters	Values
Tx/Rx Frequency	920 MHz
Time	1.087 ns
Tx Output Power	5 dBm
LO Frequency	-1 Hz
Sample Rate	1.28 MS/s
Tone Frequency	100 kHz
Number of Samples	8192
Start Trigger	Immediate
Generation Mode	Continuous

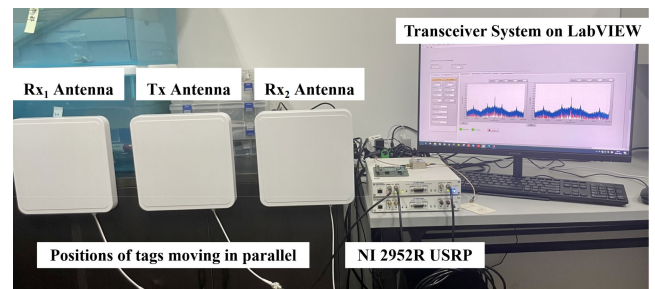


FIGURE 7. Transceiver system testing environment.

If the separation distance is too short, it will cause mutual interference. The maximum reading/writing distance of the white commercial card tag (Fig. 8. b) is not more than 1.2 m (the tag returns the most stable signal within 1m). To ensure the tag reflects signal stability when moving, it is necessary to move the tag in a parallel line from the antennas, and the vertical distance is 0.4 m. The tag is compatible with the Chinese frequency band 840 MHz - 845 MHz and 920 MHz - 925 MHz, so the operating frequency is set to 920 MHz.

B. TESTING RESULTS OF SINGLE RX ANTENNA

In order to compare the difference between dual Rx antennas and a single Rx antenna, it is necessary first to measure the signal strength received by a single antenna. Therefore, the 1T1R transceiver system (Fig. 9) must be run first. After the USRP device begins to continuously and steadily transmit the Query Command, move the tag in parallel between positions 1 to 5. Tx continuously sends the high-level carriers to power the tag and reserves the tag answer gap. The three communication cycles are obtained when the tag is placed at position 1 and position 3, respectively, as shown in Fig. 10.

Based on the sum of squares of the I and Q levels of the RN16 signal, it can be calculated that when the tag moves between positions 1-3-5 in parallel, the energy of reflected signals will go through a process: rising first and then falling. The magnitude of the energy is reversely correlated with the distance between the tag and the Rx antenna. The signal strength reaches the most robust level at position 3, as shown

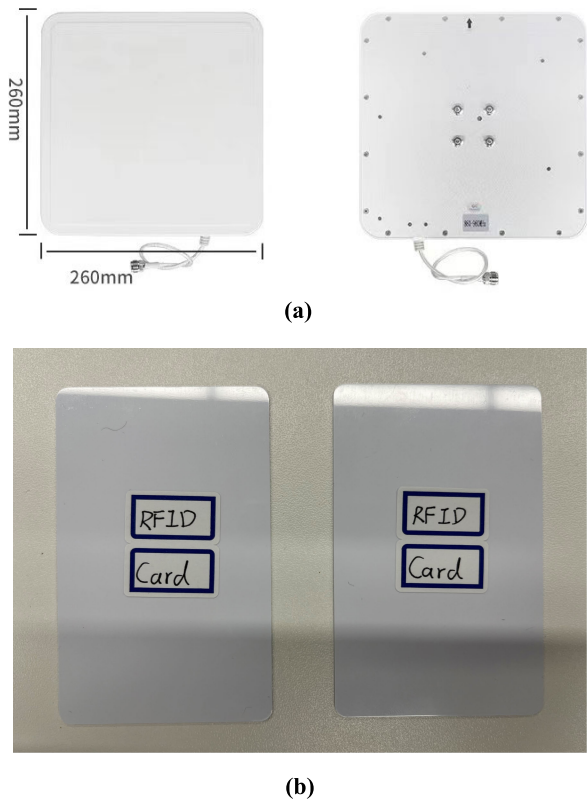


FIGURE 8. (a) The UHF RFID circularly polarized directional antenna. (b) Commercial standard white card tags.

TABLE 2. Transceiver system testing tools.

Name	Description	Performance
NI USRP-2952R	RF Signal Resource	10 MHz - 6 GHz
UHF Directional Antennas	Circularly polarized	9 dBi Gain
RFID Electronic Tag	Commercial standard card tag	Read/Write distance: 1.0 m

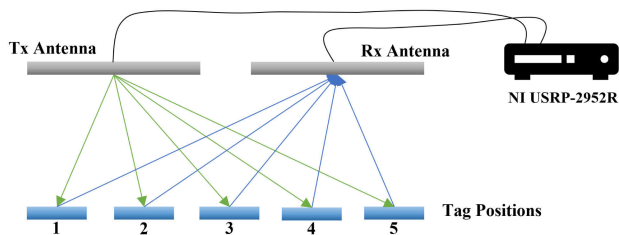


FIGURE 9. 1T1R transceiver system with tag placement.

in Fig. 11. The signal strength ranges from -35 dBm to -42 dBm. With R_{ref} being 50Ω , the voltage amplitude can be calculated accordingly:

$$V_{rms} = 3.98 \text{ mV} - 1.78 \text{ mV} = 2.20 \text{ mV} \quad (9)$$

As a result of the experiment, the maximum signal energy received by a single antenna is 2.20 mV. This is the optimal data obtained when using a single antenna for signal

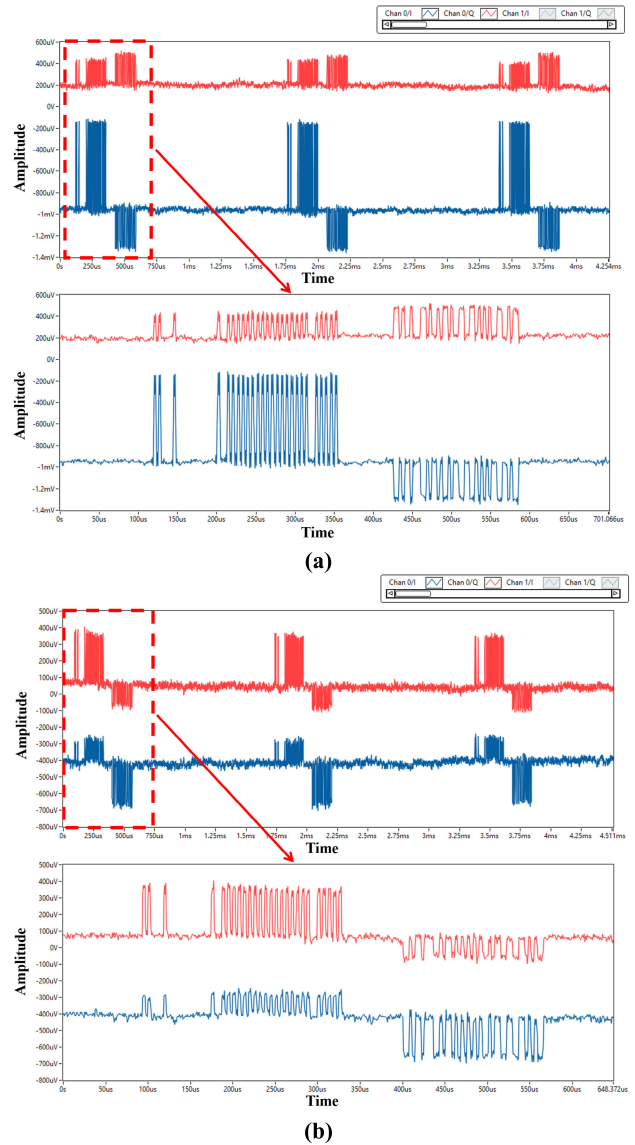


FIGURE 10. Three entire communication cycles. (a) Tag is placed at position 1 (b) Tag is placed at position 3.

receiving. This value will serve as the benchmark for subsequent 1T2R system tests.

C. TESTING RESULTS OF 1T2R TRANSCEIVER SYSTEM

Run the 1T2R system (as shown in Fig. 12) and compare it with data from a single antenna. The steps for measuring are as follows:

- 1) First, align the tag angle parallel to the antennas so that it can reflect RN16 steadily.
- 2) Then, move the tag back and forth between positions 1 to 5 at a uniform speed. During this movement, the carrier signals received by the two Rx antennas should be directly superimposed without PS.
- 3) Next, send the carriers to the down-mixer and baseband modules for demodulation, filtering, and a series of processing in the Rx part (as shown in Fig. 6. e).

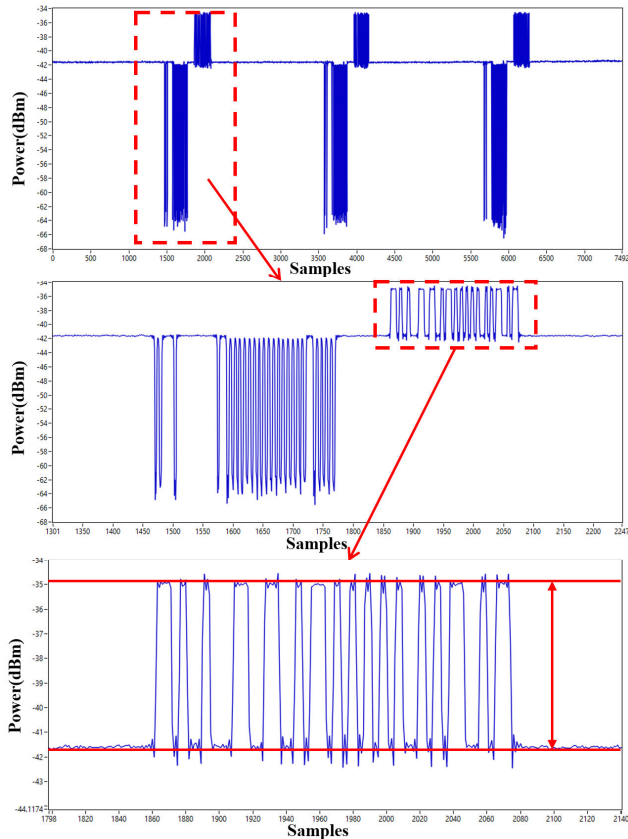


FIGURE 11. Reflected signal energy power (dBm) at tag position 3.

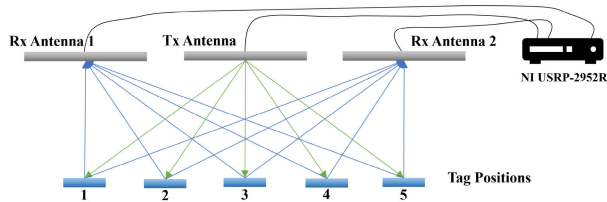


FIGURE 12. 1T2R transceiver system with tag placement.

4) Finally, the superimposed signal, $S_{combine}$, can be obtained.

When the tag travels from position 1 to 5 at a steady pace, there is a noticeable fluctuation in the amplitude of $S_{combine}$. This fluctuation follows a pattern of increase, decrease, increase, decrease, increase, and decrease, as illustrated in Fig. 13.

Fig. 14 demonstrates the exact distances between antennas and the tag. To avoid interference, it is essential to maintain a minimum distance of 10 cm between each antenna. When moving the commercial electronic tag, keep it in a parallel line from the antennas and maintain a vertical distance of 0.4 m to ensure the tag receives the Query Command and reflects RN16 signal stability. According to the theory analysis, when the distance difference of the tag from two Rx antennas satisfies (12), the reflected signal will be enhanced

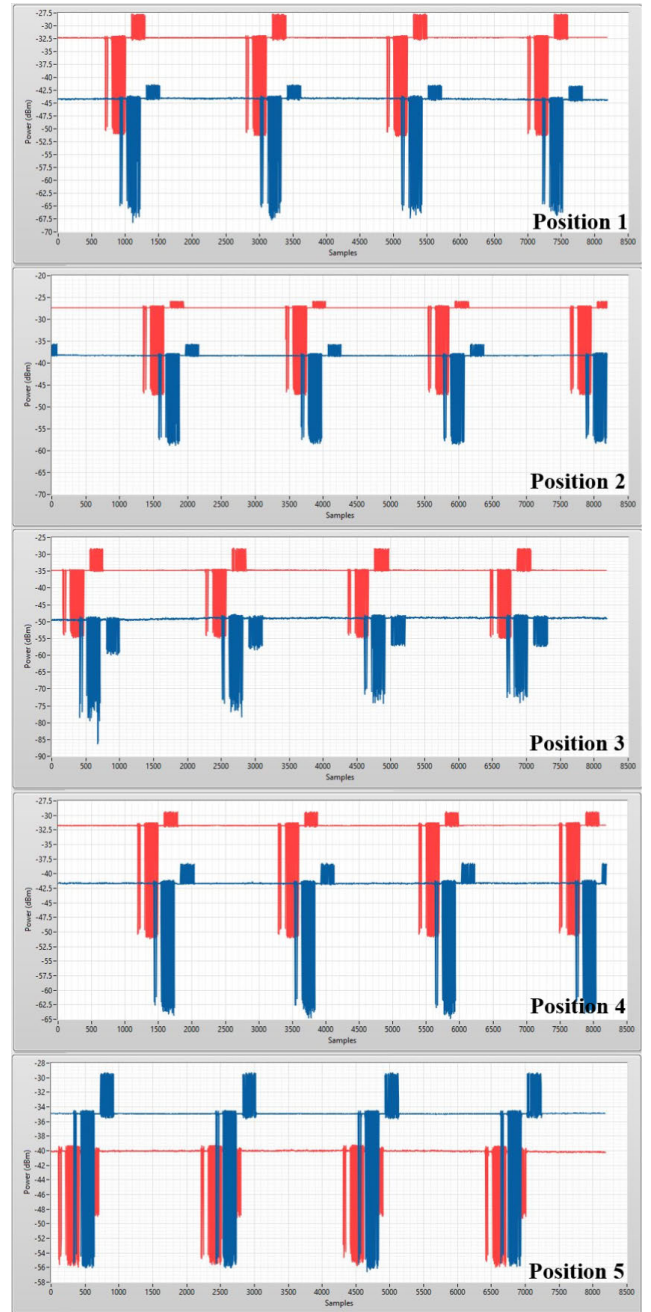


FIGURE 13. Signal energy changes when the tag moves in positions 1 to 5.

due to superposition.

$$|d_{R1} - d_{R2}| = n\lambda \quad (n = 0 \text{ or } n \in N) \tag{10}$$

$$\lambda = \frac{c}{f} = 3 \times 10^8 \text{ m/s} / 920 \text{ MHz} \approx 0.326 \text{ m} \tag{11}$$

$$|d_{R1} - d_{R2}| = n \cdot \lambda \approx n \cdot 0.326 \text{ m} \quad (n = 0 \text{ or } n \in N) \tag{12}$$

Position 1 is perpendicular to the center point of Rx antenna 1, as shown in Fig. 14. When the tag reaches position 1, its distances from two Rx antennas are as follows:

$$d_{R1} = 0.4 \text{ m} \tag{13}$$

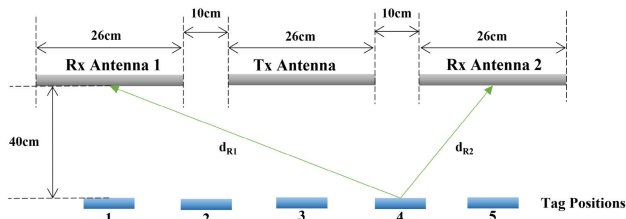


FIGURE 14. Exact distances between antennas and the tag.

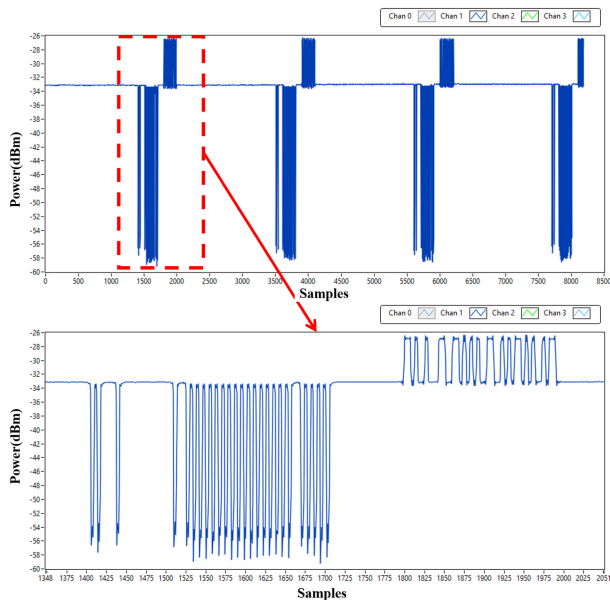


FIGURE 15. Superimposed power of the two signals when the tag is at position 3.

$$d_{R2} = \sqrt{0.4^2 + 0.72^2} \approx 0.82 \text{ m} \quad (14)$$

$$d_{R1} - d_{R2} = 0.42 \text{ m} > \lambda \quad (15)$$

Position 3 is perpendicular to the center point of the Tx antenna. When the tag moves to position 3, it is at an equal distance from both Rx antennas, which gives:

$$d_{R1} - d_{R2} = 0 \quad (16)$$

Therefore, as the tag moves from position 1 to 3, it goes through a process: the level amplitude of the signal rapidly increases to a maximum, then decreases to a negligible level. It reaches a maximum level amplitude again at position 3. When the tag moves to position 3, the signal strength is superimposed to the highest value (Fig. 15). The power range of the RN16 signal is -27.5 dBm to -33.5 dBm , and the voltage amplitude is calculated as:

$$V_{rms} = 9.43 \text{ mV} - 4.73 \text{ mV} = 4.70 \text{ mV} \quad (17)$$

Obviously, the reflected signal energy is significantly enhanced by the carrier superposition. In moving the tag from position 1 to position 5, $S_{combine}$ will experience more than two reduction changes to zero because of coherent superposition. Therefore, the received signal needs to be phase-shifted to ensure the reflected signal is continuously in

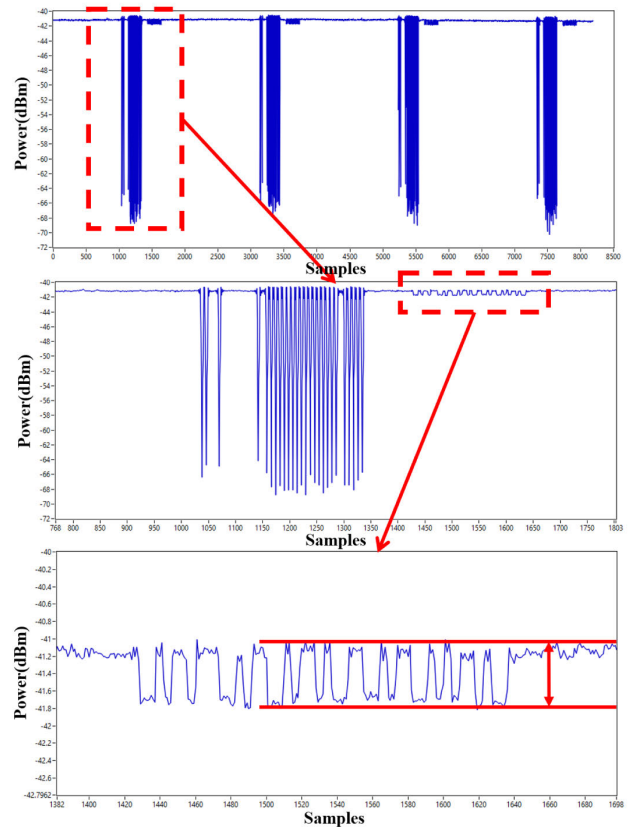


FIGURE 16. The signal strength of the superimposed signal is infinitely close to the nadir.

a superimposed and enhanced state. It has essential research significance for improving the sensitivity of BCS.

IV. ACHIEVEMENT OF HIGH SENSITIVITY

After analyzing the test results of 1T1R and 1T2R systems, it was discovered that the voltage amplitude of a single Rx antenna is 2.20 mV . Under ideal conditions, when two Rx antennas are used, the maximum voltage amplitude of the combined signal ($S_{combine}$) is 4.70 mV .

Hence, the main tasks to be accomplished in this section are outlined below:

- 1) According to the fluctuation pattern of the combined signal, fix the tag at locations where the superimposed signal is offset and weakened;
- 2) Add adjustable modules of phase shifting to the two Rx parts on LabVIEW, respectively;
- 3) In the Rx baseband module, the received signal undergoes filtering and demodulation. Subsequently, phase shifting (PS_1) on the carrier signal is performed to test the signal energy of $S_{combine}$;
- 4) Compare the phase-shifted measurement results with the voltage amplitude of 4.70 mV obtained from the dual-antenna signal receiving under ideal conditions.

In this way, it is possible to verify whether the PS process of two reflected carriers can contribute sensitivity improvement to the BCS.

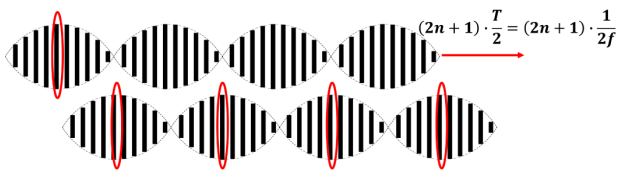


FIGURE 17. Phase shift of the reflected signal carriers.

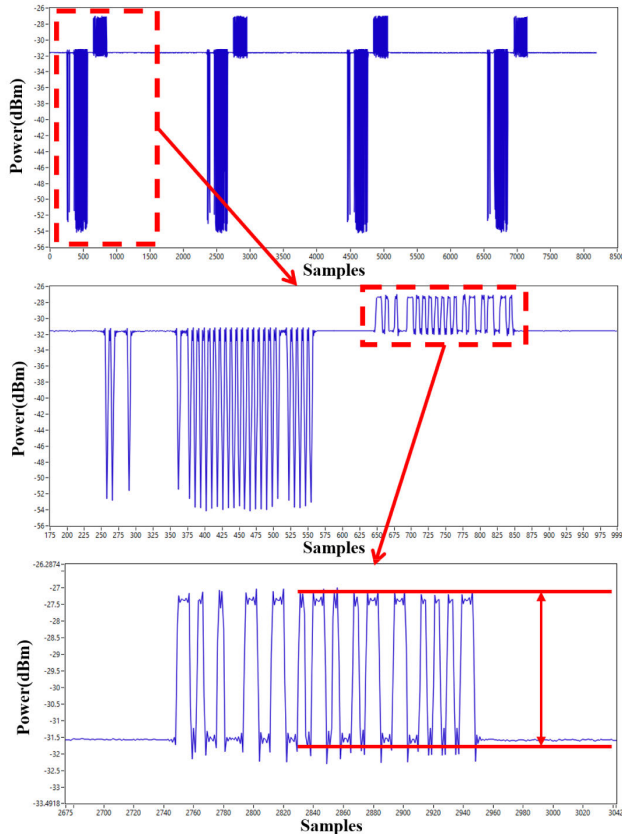


FIGURE 18. Power value after superposition of two reflected signals at a phase shift $T/2$.

When moving the tag, the reflected signal observed from the LabVIEW window is affected by many factors, such as speed, distance, and electromagnetic interference, which leads $S_{combine}$ to a dynamic change. When the power of $S_{combine}$ is zero, it is necessary to exclude the situation in the system that does not establish communication with the tag. Accordingly, it is more reasonable to choose the locations where the power value of $S_{combine}$ is very weak but can be observable as the positions for the PS_1 comparison experiment.

After adjusting, at this position point, we can read the RN16 signal power range is -41.9 dBm to -41.7 dBm (Fig. 16), then calculate the voltage amplitude as follows:

$$V_{rms} = 1.84 \text{ mV} - 1.80 \text{ mV} = 0.04 \text{ mV} \approx 0 \quad (18)$$

The data at this position point is used for subsequent PS_1 comparison experiments. Add a PS_1 to one of the Rx channels through the Phase Shifter module. It is supposed to be added

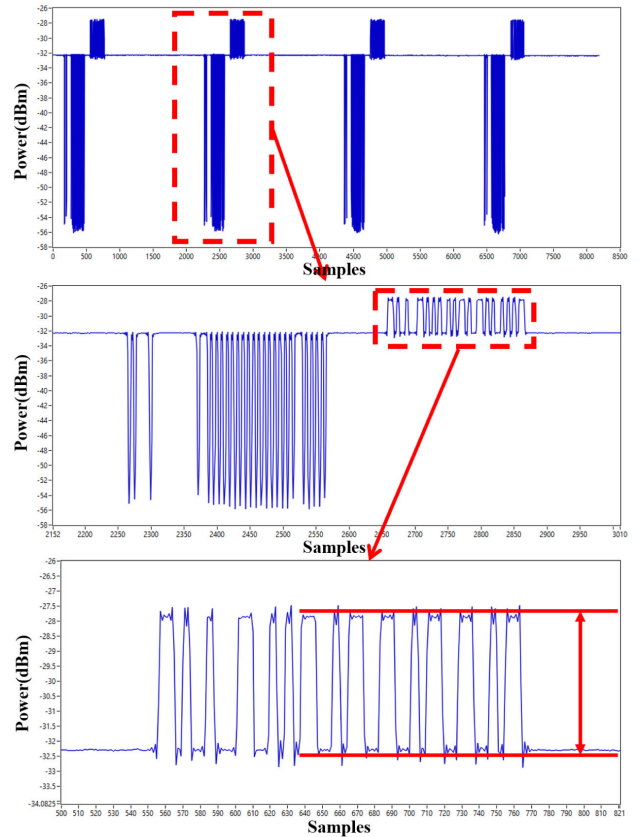


FIGURE 19. Power value after superposition of two reflected signals at a phase shift $7 \cdot T/2$.

before the down-mixing and filtering process. According to TABLE 1, the RF system is set to 920 MHz, so the modulated carrier oscillation period is $1/920 \text{ MHz} \approx 1.087 \text{ ns}$. Thus, the added PS_1 must satisfy the following conditions (19) to achieve the carrier superimposition (Fig. 17):

$$PS = (2n + 1) \cdot \frac{T}{2} \approx (2n + 1) \cdot 0.543 \text{ ns} \quad (19)$$

Firstly, take $n = 1$, then one of the received carriers is phase-shifted $T/2$ to obtain the superimposed signal $Combine_1$ (Fig. 18). Then, the signal power range of RN16 can be read out -27 dBm to -32 dBm. Convert the unit to calculate the voltage amplitude as:

$$V_{rms} = 9.99 \text{ mV} - 5.62 \text{ mV} = 4.37 \text{ mV} \quad (20)$$

In order to enhance the accuracy of the testing results, $n = 3$ is performed as a phase shift of $7 \cdot T/2$. At this time, the reflected superimposed signal $Combine_1$ is as shown in Fig. 19. To read out the signal power range is -27.5 dBm to -32.5 dBm, the voltage amplitude can be calculated as:

$$V_{rms} = 9.43 \text{ mV} - 5.30 \text{ mV} = 4.13 \text{ mV} \quad (21)$$

The measurement result of 4.37 mV is close to the value obtained at a phase shift of $T/2$ when $n = 1$. Under the same testing conditions, both 4.37 mV and 4.13 mV are close to the highest value of 4.70 mV and significantly higher than the

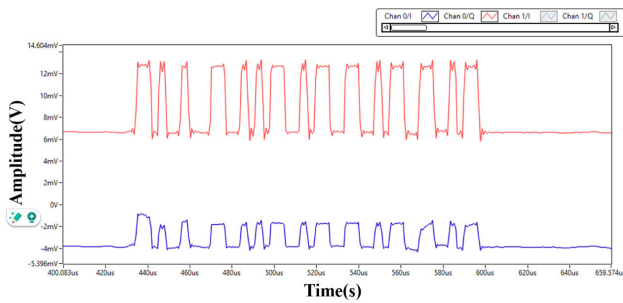


FIGURE 20. The demodulated and decoded 16-bit pseudorandom sequence (RN16 signal) reflected from tags.

highest value of 2.20 mV obtained with a single Rx antenna, which is almost twice as much. Hence, it is evident that the signal enhancement is achieved by PS_1 . When comparing 4.37 mV with 2.20 mV, the signal gain obtained is calculated as follows:

$$\begin{aligned} G_{PS} &= 4.37 \text{ mV} - 2.20 \text{ mV} \\ &= (-34.18 \text{ dBm}) - (-40.14 \text{ dBm}) \\ &= 5.96 \text{ dB} \end{aligned} \quad (22)$$

To ensure the accuracy of the measurement results, the obtained data signal is demodulated and decoded. As shown in Fig. 20, it can be confirmed that the RN16 pseudorandom sequence is correct and compatible with the EPC Gen2 protocol. Moreover, the signal gain of 5.96 dB is as expected, which is a crucial aspect to consider.

Similarly, using the same approach, add PS_2 into the other Rx_2 part (Fig. 6. e) on the LabVIEW transceiver system to superimpose the two reflected signals with a phase shift of $T/2$ and $3*T/2$. A signal gain of 5.82 dB can also be achieved in the $Combine_2$ channel. The results of the experiment prove that the 1T2R transceiver designed in this study can achieve signal enhancement of the two combined channels through phase shifting, which contributes to the realization of the high sensitivity of the backscatter communication system.

V. CONCLUSION

This paper mainly researches the theoretical feasibility and practical verification of utilizing MIMO technology in a 920 MHz backscatter communication system. For this purpose, we explained the feasibility of implementing MIMO technology to backscatter communication systems based on principles and simulated it through the MATLAB model. Moreover, we built a dual-channel 1T2R transceiver system on the LabVIEW platform and conducted 1T1R and 1T2R experimental tests. Through the process of superimposing and utilizing varying phase shifts between two reflected carriers, it has been confirmed that the overall signal strength can be boosted from 2.2 mV to 4.13 mV and 4.37 mV (nearly reaching 4.70 mV in ideal conditions). This advancement increases signal strength from -40.14 dBm (when using a single Rx antenna) to -34.18 dBm (when using two Rx antennas). This improvement in signal strength can provide a gain of 5.96 dB to the backscatter communication systems.

The results of testing the other combined channel can also provide evidence of the signal enhancement.

The experimental data effectively proves that implementing MIMO technology to the receiver can efficiently improve the sensitivity of the backscatter communication systems at 920 MHz.

REFERENCES

- [1] M. Weqar, S. Mehruz, D. Gupta, and S. Urooj, "Adaptive switching based data-communication model for Internet of Healthcare Things networks," *IEEE Access*, vol. 12, pp. 11530–11548, 2024.
- [2] J. Mitsugi, O. Tokumasu, and H. Sakabe, "Two-stage harmonics rejection in FDMA backscatter communication system using FFT filterbank," *IEEE J. Radio Freq. Identificat.*, vol. 7, pp. 518–527, 2023.
- [3] R. Y. Aburasain, "Enhanced black widow optimization with hybrid deep learning enabled intrusion detection in Internet of Things-based smart farming," *IEEE Access*, vol. 12, pp. 16621–16631, 2024.
- [4] S. Yang, M. Crisp, R. V. Penty, and I. H. White, "RFID system exploiting large metal objects as near field UHF RFID antennas," in *Proc. IEEE Int. Conf. RFID (RFID)*, May 2017, pp. 96–102.
- [5] N. A. Ugochukwu, S. B. Goyal, A. S. Rajawat, C. Verma, and Z. Illés, "Enhancing logistics with the Internet of Things: A secured and efficient distribution and storage model utilizing blockchain innovations and inter-planetary file system," *IEEE Access*, vol. 12, pp. 4139–4152, 2024.
- [6] S. Yang and L. Hanzo, "Fifty years of MIMO detection: The road to large-scale MIMOs," *IEEE Commun. Surveys Tuts.*, vol. 17, no. 4, pp. 1941–1988, 4th Quart., 2015.
- [7] P. K. Udayaprasad, J. Shreyas, N. N. Srinidhi, S. M. D. Kumar, P. Dayananda, S. S. Askar, and M. Abouhawwash, "Energy efficient optimized routing technique with distributed SDN-AI to large scale I-IoT networks," *IEEE Access*, vol. 12, pp. 2742–2759, 2024.
- [8] S. F. Ahmed, M. S. B. Alam, S. Afrin, S. J. Rafa, S. B. Taher, M. Kabir, S. M. Mueyen, and A. H. Gandomi, "Toward a secure 5G-enabled Internet of Things: A survey on requirements, privacy, security, challenges, and opportunities," *IEEE Access*, vol. 12, pp. 13125–13145, 2024.
- [9] E. Denicke, H. Hartmann, B. Geck, and D. Manteuffel, "MIMO backscatter channel and data transmission measurements," in *Proc. 47th Eur. Microw. Conf. (EuMC)*, Oct. 2017, pp. 723–726.
- [10] P. Chaudhary, A. Yadav, A. Kumar, K. Patel, R. K. Arya, and M. Ali, "Ring with rectangular StubMIMO antenna for RFID applications," in *Proc. IEEE Int. Conf. RFID Technol. Appl. (RFID-TA)*, Oct. 2021, pp. 227–230.
- [11] P. Bienkowski, B. Zubrzak, P. Sobkiewicz, K. Bechta, and M. Rybakowski, "Simplified methodology of electromagnetic field measurements in the vicinity of 5G massive MIMO base station for environmental exposure assessment," *IEEE Access*, vol. 12, pp. 8071–8080, 2024.
- [12] T. Govindan, S. K. Palaniswamy, M. Kanagasabai, S. Kumar, T. R. Rao, and L. Kannappan, "RFID-band integrated UWB MIMO antenna for wearable applications," in *Proc. IEEE Int. Conf. RFID Technol. Appl. (RFID-TA)*, Oct. 2021, pp. 199–202.
- [13] R. Fara, N. Bel-Haj-Maati, D.-T. Phan-Huy, N. Malhouroux, and M. Di Renzo, "First experimental evaluation of ambient backscatter communications with massive MIMO reader," in *Proc. IEEE 31st Annu. Int. Symp. Pers., Indoor Mobile Radio Commun.*, Aug. 2020, pp. 1–6.
- [14] C. Munusami and R. Venkatesan, "A compact boat shaped dual-band MIMO antenna with enhanced isolation for 5G/WLAN application," *IEEE Access*, vol. 12, pp. 11631–11641, 2024.
- [15] Y. Li and C. Zhong, "Capacity for correlated MIMO backscatter systems," in *Proc. IEEE/CIC Int. Conf. Commun. Workshops China (ICCC Workshops)*, Aug. 2019, pp. 54–58, doi: 10.1109/ICCCCHINAW.2019.8849972.
- [16] S. Zheng, R. Liu, J. Sun, H. Dang, and X. Tan, "Simulation modeling and real measurement for lunar surface backscattering coefficient," in *Proc. Cross Strait Quad-Regional Radio Sci. Wireless Technol. Conf. (CSQRWC)*, Jul. 2019, pp. 1–2.
- [17] C. He, Z. J. Wang, C. Miao, and V. C. M. Leung, "Block-level unitary query: Enabling orthogonal-like space-time code with query diversity for MIMO backscatter RFID," *IEEE Trans. Wireless Commun.*, vol. 15, no. 3, pp. 1937–1949, Mar. 2016.
- [18] K. Tang, M. Wang, M. Liu, C. Zhang, S. Xu, S. Ji, S. Lai, N. Yan, H. Min, and J. Mitsugi, "A highly integrated passive wireless sensing system with synchronized data streaming of multiple tags," *IEEE Internet Things J.*, vol. 9, no. 17, pp. 15525–15537, Sep. 2022.

- [19] C. He, H. Luan, X. Li, C. Ma, L. Han, and Z. Jane Wang, "A simple, high-performance space-time code for MIMO backscatter communications," *IEEE Internet Things J.*, vol. 7, no. 4, pp. 3586–3591, Apr. 2020.
- [20] M. Kaushik, J. K. Dhanoa, and M. K. Khandelwal, "Meander line based two port MIMO small antenna for UHF RFID and Sub-6 GHz applications," in *Proc. IEEE Int. Conf. RFID Technol. Appl. (RFID-TA)*, Oct. 2021, pp. 219–222.
- [21] U. Sharma, G. Srivastava, and M. K. Khandelwal, "Small MIMO antenna with circular polarization for UHF RFID, PCS and 5G applications," in *Proc. IEEE Int. Conf. RFID Technol. Appl. (RFID-TA)*, Oct. 2021, pp. 223–226.
- [22] T. Wu, M. Jiang, Q. Zhang, Q. Li, and J. Qin, "Beamforming design in multiple-input-multiple-output symbiotic radio backscatter systems," *IEEE Commun. Lett.*, vol. 25, no. 6, pp. 1949–1953, Jun. 2021.
- [23] R. Luo, H. Yang, C. Meng, and X. Zhang, "A novel SR-DCSK-based ambient backscatter communication system," *IEEE Trans. Circuits Syst. II: Exp. Briefs*, vol. 69, no. 3, pp. 1707–1711, Mar. 2022.
- [24] J. Wei and X. Tian, "Capacity analysis of frequency shift based backscatter communication system," in *Proc. 3rd Int. Conf. Comput. Commun. Syst. (ICCCS)*, Apr. 2018, pp. 353–357.
- [25] H. Lin, X. Yang, L. Ge, Y. Li, S.-W. Wong, and K. W. Tam, "Self-decoupling antennas for MIMO UHF RFID systems," in *Proc. IEEE Int. Conf. RFID Technol. Appl. (RFID-TA)*, Oct. 2021, pp. 275–277.
- [26] M. R. ur Rehman, S. J. Oh, I. Ali, M. Asif, and K.-Y. Lee, "Modeling of SWIPT system with ASK modulation in LabVIEW," in *Proc. Int. Conf. Electron., Inf., Commun. (ICEIC)*, Jan. 2019, pp. 1–4.
- [27] S. Jadon, A. Rao, N. Jagadish, S. Nadakatti, T. R., and P. B. Honnavalli, "Blockchain in the electronics industry for supply chain management: A survey," *IEEE Access*, vol. 12, pp. 7089–7120, 2024.
- [28] A. R. Unterhuber, S. Iliev, and E. Biebl, "Interferences and shadowing in multi-lane UHF RFID-based vehicle identification systems," in *Proc. IEEE Int. Conf. RFID Technol. Appl. (RFID-TA)*, Oct. 2021, pp. 153–156.
- [29] W. Wang, "A IoT-based framework for cross-border E-commerce supply chain using machine learning and optimization," *IEEE Access*, vol. 12, pp. 1852–1864, 2024.



SIJIA LAI received the B.S. degree from the Department of Communication Engineering, Zhengzhou University, Zhengzhou, China, in 2015, and the M.S. degree in wireless communication systems from The University of Sheffield, Sheffield, U.K., in 2017. She is currently pursuing the Ph.D. degree with the State Key Laboratory of ASIC and System, Fudan University, Shanghai, China.

From 2019 to 2020, she was a Visiting Ph.D. Scholar at the Department of Electrical Engineering, University of California, Los Angeles (UCLA), Los Angeles, CA, USA. Her research interests include low-power digital baseband and high-sensitivity receiver in the RFID and backscatter communication systems.



YUXIAO ZHAO (Member, IEEE) received the B.Sc. degree (Hons.) from Harbin Institute of Technology, in 2019. He is currently pursuing the Ph.D. degree with the State Key Laboratory of ASIC and System, Fudan University, Shanghai, China.

His research interests include ultra-low-power receivers, frequency synthesizers, and analog/mixed-signal circuits and systems.



MENG LIU was born in Cangzhou, China, in 1998. He received the B.S. degree in microelectronics from Xidian University, Xi'an, China, in 2020. He is currently pursuing the Ph.D. degree with the School of Microelectronics, Fudan University, Shanghai, China.

His current research interests include low power mixed-signal integrated circuit design, power management, and ultra-low power transceiver design.



SHENGLIANG XU received the B.S. degree in optoelectronics information science and engineering from Tianjin Polytechnic University, Tianjin, China, in 2017, and the M.E. degree from the Department of Microelectronic, Fudan University, Shanghai, China, in 2020.

His research interests include RFID anticollision algorithm research and analog circuit design.



KUANGFENG TANG received the M.S. degree in electronic science and technology from Nankai University, Tianjin, China, in 2018, and the Ph.D. degree in microelectronics from the State Key Laboratory of ASIC and System, Fudan University, Shanghai, China, in 2023.

His research interests include high-speed high-precision ADC, backscatter sensing system and high-sensitivity wireless receiver design, and RF frontend circuits design and analog baseband circuit design.



HAO MIN (Member, IEEE) received the B.S. and M.S. degrees in electrical engineering and the Ph.D. degree in material science from Fudan University, Shanghai, China, in 1985, 1988, and 1991, respectively. From 1991 to 1998, he was an Associate Professor at the Application Specific Integrated Circuit (ASIC) and Systems State Key Laboratory, Fudan University. From 1995 to 1998, he was a Visiting Associate Professor at the Department of Electrical Engineering, Stanford

University, Stanford, CA, USA, where he was involved in low-power mixed-signal very large-scale integration (VLSI) design, especially in the design and characterizing of CMOS image sensors. Since 1998, he has been a Professor and the Director of the ASIC and System State Key Laboratory, Fudan University. In 2002, he joined with the Auto-ID Center of China. He is currently a Research Director of the Auto-ID Laboratory, Fudan University. He has authored or co-authored over 50 papers in journals and conferences. He has ten patents pending. His current research interests include VLSI architecture, RF and mixed-signal integrated circuit design, digital signal processing, and image procession.

...